Proceedings of IMECE 2005
ASME International Mechanical Engineering Congress and Exposition
November 5-11, 2005, Orlando, Florida, USA

IMECE2005-81780

Effects of Various Modeling Schemes on Mist Film Cooling Simulation

Xianchang Li and Ting Wang
Energy Conversion & Conservation Center
University of New Orleans
New Orleans, LA 70148-2220

Abstract

Numerical simulation is performed in this study to explore film-cooling enhancement by injecting mist into the cooling air with a focus on investigating the effect of various modeling schemes on the simulation results. The effect of turbulence models, dispersed-phase modeling, inclusion of different forces (Saffman, thermophoresis, and Brownian), trajectory tracking, and mist injection scheme is studied. The effect of flow inlet boundary conditions (with/without air supply plenum), inlet turbulence intensity, and the near-wall grid density on simulation results is also included. Using a 2-D slot film cooling simulation with a fixed blowing angle and blowing ratio shows a 2% mist injected into the cooling air can increase the cooling effectiveness about 45%. The RNG k-ε model, RSM and the standard k-ε turbulence model with the enhanced wall treatment produce consistent and reasonable results while the turbulence dispersion has a significant effect on mist film cooling through the stochastic trajectory calculation. The thermophoretic force slightly increases the cooling effectiveness, but the effect of Brownian force and Saffman lift is imperceptible. The cooling performance is affected negatively by the plenum in this study, which alters the velocity profile and turbulence intensity at the jet exit plane. The results of this paper can serve as the qualification reference for future more complicated studies including 3-D cooling holes, different blowing ratios, various density ratios, and rotational effect.

Keywords: film cooling, gas turbine cooling, mist cooling, two-phase flow simulation

Nomenclature

b	slot width (m)
C	concentration (kg/m^3)
c_p	specific heat (J/kg-K)
D	mass diffusion coefficient (m^2/s)
d	droplet diameter (m)
F	force (N)
k	turbulence kinetic energy (m^2/s^2)
k_c	mass transfer coefficient (m/s)
h	convective heat transfer coefficient (W/m^2-K)
h_{fg}	latent heat (J/kg)
M	blowing ratio, $(\rho u)_c/(\rho u)_g$
m	mass (kg)
Nu	Nusselt number, hd/λ
P	pressure (N/m^2)
Pr	Prandtl number, ν/α
Re	Reynolds number, ud/ν
Sc	Schmidt number (ν/D)
Sh	Sherwood number ($k_c d/D$)
T	temperature (K, ^{o}F)
t	time (s)
u	streamwise velocity component (m/s)
u', T', C'	turbulence fluctuation terms
v	spanwise velocity component (m/s)
x, y	coordinates

Greek

α	thermal diffusivity (m^2/s)
ε	turbulence dissipation rate (m^2/s^3)
η	film cooling effectiveness, $(T_g-T_c)/(T_g-T_{aw})$
λ	heat conductivity (W/m-K)
μ	dynamic viscosity (kg/m-s)
ν	kinematic viscosity (m^2/s)
ρ	density (kg/m^3)
τ	stress tensor (kg/m-s^2)

Subscript

aw	adiabatic wall
c	coolant or jet flow
g	hot gas/air
p	particle or droplet
t	turbulent
0	air film cooling without mist
∞	far away from droplets

Introduction

For more than half a century [1-2], air film cooling has been commonly applied to cool gas turbine hot components such as combustor liners, combustor transition pieces, turbine vanes (nozzles) and blades (buckets). Numerous studies have been performed to make film cooling more effective by optimizing the compound injection angles and blowing ratios and designing different injection hole configurations.

Open literature shows that the optimal injection angle of forward inclination is about 30~35°. Jia et al. [3] verified that the recirculation bubble downstream the jet vanishes when the angle is 30° or less. The injection angle in Bell et al. [4] and Brittingham and Leylek [5] is 35°. Taslim and Khanicheh [6] conducted experimental and numerical studies with an injection angle of 25°. The blowing ratio is another important parameter in film cooling. As found in [3], it has a large effect on the size of recirculation. Kwak and Han [7] measured heat transfer coefficients and film-cooling effectiveness on a gas turbine blade tip. Their results showed that heat transfer coefficient decreased as blowing ratio increased, while film effectiveness increased. Mayhew et al. [8] measured the adiabatic cooling effectiveness of film cooling with compound angle holes using thermochronic liquid crystal. Their photographs show that large blowing ratios lower the cooling performance.

Since the mixing between the coolant and main flow is partially controlled by turbulence diffusion, the inlet turbulence intensity of coolant jet also affects the film cooling. As shown in Mayhew et al. [8], low inlet turbulence intensity keeps the coolant close to the wall when the blowing ratio is low; while high inlet turbulence intensity helps bring the coolant back to the wall when the blowing ratio is high. To consider the effect of upstream flow conditions on film cooling, an inlet plenum as well as the flow arrangement is included in numerical studies by Brittingham and Leylek [5], Adami et al. [9], etc. It is concluded that an accurate prediction of coolant discharge and wall coverage of cooling film requires computation of flow field in the cooling air supply plenum and duct.

Many studies have been conducted on the shaped holes with various configurations. For example, Bell et al. [4] found laterally diffused compound angle holes and forward diffused compound angle holes produce higher effectiveness over much wider ranges of blowing ratio and momentum flux ratio compared to the other three simple-angle configurations tested. Brittingham and Leylek [5] concluded that the compound-angle shaped holes could be designed to eliminate crossflow line-of-sight between adjacent holes, and thus somewhat mimic slot-jet performance. To eliminate nonuniform cooling pattern inherent in the discrete injection holes, Wang et al. [10] conducted experiments by embedding the discrete injection holes in a slot recessing beneath the surface. Premixing inside the slot makes the slot film cooling more uniform than discrete injection holes.

Although these technologies can continuously improve the performance of conventional air film cooling, the increased net benefits seem to be incremental and approaching their limit. In view of the high contents of H_2 and CO in the synthetic fuels for next generation turbines, the increased flame temperatures and flame speeds from those of natural gas combustion will make gas turbine cooling more difficult and more important. Therefore, development of new cooling techniques is essential for surpassing current limits. One potential new cooling technique is to inject small amounts of tiny water droplets (mist) into the cooling air to enhance the cooling performance. The key mist cooling enhancement mechanism is attributed to the latent heat that droplet evaporation will absorb when moving along the coolant air. The second cooling enhancement mechanism is contributed by direct contact between water droplet and the wall. Other minor cooling enhancement mechanisms include increased temperature gradient and augmented mixing induced by droplet-air interactions. Furthermore, continuous droplets evaporation can last longer and go farther into the downstream region where single-phase air film cooling becomes less effective.

Mist has been used to enhance heat transfer in gas turbine systems in different ways. Gas turbine inlet air fog cooling [11] is a common application where the droplets evaporate to lower the compressor air inlet temperature until the relative humidity reaches 100%. In addition, fog overspray is used in industry to provide evaporative cooling inside the compressor. Petr [12] reported the results of thermodynamic analysis of the gas turbine cycle with wet compression based on detailed simulation of a two-phase compression process. In 1998, Nirmalan et al. [13] applied water/air mixture as the impingement coolant to cool gas turbine vanes. To explore an innovative approach to cooling future high-temperature gas turbines, the authors' research group has conducted a series of mist/steam cooling experimental studies by injecting 7 μm (average diameter) of water droplets into steam flow, e.g., [14-17]. For a straight tube [14], the highest local heat transfer enhancement of 200% was achieved with 1~5% (weight) mist, and the average enhancement was 100%. In a 180° tube bend [15], the overall cooling enhancement ranged from 40% to 300% with the maximum local cooling enhancement being over 800%, which occurred at about 45° downstream of the inlet of the test section. For jet impingement cooling over a flat surface [16], a 200% cooling enhancement was shown near the stagnation point by adding 1.5% mist (in mass). In jet impingement on a concave surface [17], enhancements of 30 to 200% were achieved within five-slot distance with 0.5% (weight) mist.

Besides experiments, numerical simulation is frequently used to study film cooling. Jia et al. [3] employed the V2F k-ε turbulence model to investigate slot jet film cooling. The standard k-ε model with generalized wall function was used by Brittingham and Leylek [5] to simulate film cooling with compound-angle shaped holes. Taslim and Khanicheh [6] also used the standard k-ε model with generalized wall function in their study. Heidmann et al. [18] employed a k-ω model, which does not require a specified distance to the wall for the near-wall grids. Tyagi and Acharya [19] used the large eddy simulation (LES) to reveal the anisotropic characteristics in the wake region of the cooling jet.

To simulate the flow and heat transfer of a discrete phase, such as droplets in mist film cooling, one approach is to track the particles in a Lagrangian frame of reference, and at the same time compute the heat transfer between the discrete phase and the continuous flow. The effect of discrete phase on flow and heat transfer of the continuous phase is incorporated as a source term to the governing equations. The Lagrangian method has been used in many studies such as dispersion of post-dryout dispersed flow [20], evaporating droplets in a swirling jet [21], and evaporating spray in turbulent gas flow [22]. Li and Wang [23] conducted a numerical simulation of mist film cooling using the standard k-ε turbulence model with enhanced wall function. Three different holes are used in their study including a 2-D slot, a round hole, and a fan-shaped diffusion hole. A comprehensive study is performed on the effect of flue gas temperature, blowing angle, blowing ratio, mist injection rate, and droplet size on the cooling effectiveness with 2-D cases. Significant cooling enhancements (30~50%) were predicted.

Since the accuracy and validity of simulation depends on the accuracy of numerical modeling, this paper focuses on investigating the various modeling schemes on the simulated results of mist film cooling, including effects of turbulence models, different flow-droplet interactions (Saffman force, Brownnian lift, and thermophoresis), discrete-phase modeling, mist injection locations, and trajectory tracking. The results of this paper will serve as the qualification reference for more complicated studies including 3-D cooling holes, various blowing ratios, various density ratios, and rotational effect.

Numerical Model

Geometrical Configuration

A 2-D slot is selected for this study. Its configuration and the main dimensions are shown in Fig. 1. The slot width (b) is 4 mm. The injection angle is 35°, which is considered as the optimal value by [4, 5]. The length of the film slot is 3b. The computational domain has a length of 80b and a height of 20b. The slot jet is set to 20b from the entrance of the mainstream. To study the effect of upstream conditions of coolant on the film cooling performance, a 7.0b×3.5b extended air supply plenum upstream of the film cooling slot is added later. The cooling air enters the plenum parallel to the main flow.

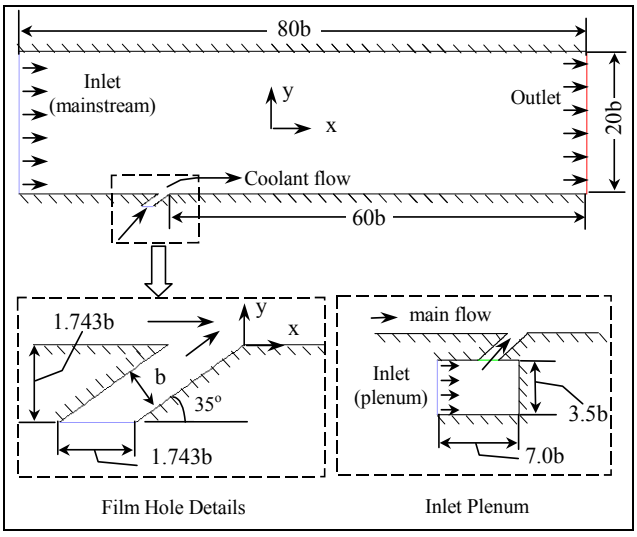

Figure 1 Computational Domain

Governing Equations

The 2-D, time-averaged, steady state Navier-Stokes equations as well as equations for mass, energy and species transport are solved. The governing equations for conservation of mass, momentum, and energy are given as:

$$\frac{\partial}{\partial x_i}(\rho u_i) = S_m \tag{1}$$

$$\frac{\partial}{\partial x_i}(\rho u_i u_j) = \rho \vec{g}_j - \frac{\partial P}{\partial x_j} + \frac{\partial}{\partial x_i}\left(\tau_{ij} - \rho\overline{u'_i u'_j}\right) + F_j \tag{2}$$

$$\frac{\partial}{\partial x_i}(\rho c_p u_i T) = \frac{\partial}{\partial x_i}\left(\lambda \frac{\partial T}{\partial x_i} - \rho c_p \overline{u'_i T'}\right) + \mu\Phi + S_h \tag{3}$$

where τ_{ij} is the symmetric stress tensor defined as

$$\tau_{ij} = \mu\left(\frac{\partial u_j}{\partial x_i} + \frac{\partial u_i}{\partial x_j} - \frac{2}{3}\delta_{ij}\frac{\partial u_k}{\partial x_k}\right). \tag{4}$$

The source terms (S_m, F_j and S_h) are used to include the contributions from the dispersed phase. $\mu\Phi$ is the viscous dissipation and λ is the heat conductivity.

In mist film cooling, water droplets evaporate and the vapor diffuses into its surrounding flow. The flow mixture consists of three main components: water vapor (H_2O), oxygen (O_2) and nitrogen (N_2). The equation for species transport is

$$\frac{\partial}{\partial x_i}(\rho u_i C_j) = \frac{\partial}{\partial x_i}\left(\rho D_j \frac{\partial C_j}{\partial x_i} - \rho\overline{u'_i C'_j}\right) + S_j, \tag{5}$$

where C_j is the mass fraction of the species (j) in the mixture, and S_j is the source term for this species. D_j is the diffusion coefficient.

Notice the terms of $\rho\overline{u'_i u'_j}$, $\rho c_p\overline{u'_i T'}$, and $\rho\overline{u'_i C'_j}$ represent the Reynolds stresses, turbulent heat fluxes and turbulent concentration (or mass) fluxes, which should be modeled properly for a turbulent flow. The Reynolds number of the main flow (based on the duct height and the inlet condition specified later) is about 30,000 in this study. Therefore, turbulence model needs to be included.

Turbulence Models

Standard k-ε Model – The standard k-ε model, which, based on the Boussinesq hypothesis, relates the Reynolds stresses to the mean velocity as

$$-\rho\overline{u'_i u'_j} = \mu_t\left(\frac{\partial u_i}{\partial x_j} + \frac{\partial u_j}{\partial x_i}\right) - \frac{2}{3}\rho k\delta_{ij} \tag{6}$$

where k is the turbulent kinetic energy, and μ_t is the turbulent viscosity given by

$$\mu_t = \rho C_\mu k^2/\varepsilon \tag{7}$$

where C_μ is a constant and ε is the dissipation rate. The equations for the turbulent kinetic energy (k) and the dissipation rate (ε) are:

$$\frac{\partial}{\partial x_i}(\rho u_i k) = \frac{\partial}{\partial x_i}\left[\left(\mu + \frac{\mu_t}{\sigma_k}\right)\frac{\partial k}{\partial x_i}\right] + G_k - \rho\varepsilon. \tag{8}$$

$$\frac{\partial}{\partial x_i}(\rho u_i \varepsilon) = \frac{\partial}{\partial x_i}\left[\left(\mu + \frac{\mu_t}{\sigma_\varepsilon}\right)\frac{\partial \varepsilon}{\partial x_i}\right] + C_{1\varepsilon}G_k\frac{\varepsilon}{k} - C_{2\varepsilon}\rho\frac{\varepsilon^2}{k}. \tag{9}$$

The term G_k is the generation of turbulence kinetic energy due to the mean velocity gradients.

The turbulent heat flux and mass flux can be modeled with the turbulent heat conductivity (λ_t) and the turbulent diffusion coefficient (D_t), respectively.

$$\rho c_p\overline{u'_i T'} = -\lambda_t\frac{\partial T}{\partial x_i} = -c_p\frac{\mu_t}{Pr_t}\frac{\partial T}{\partial x_i}, \tag{10}$$

$$\rho\overline{u'_i C'} = -\rho D_t\frac{\partial C}{\partial x_i} = -\frac{\mu_t}{Sc_t}\frac{\partial C}{\partial x_i}. \tag{11}$$

The constants $C_{1\varepsilon}$, $C_{2\varepsilon}$, C_μ, σ_k, and σ_ε used are: $C_{1\varepsilon}$ = 1.44, $C_{2\varepsilon}$ = 1.92, C_μ = 0.09, σ_k = 1.0, σ_ε =1.3 [24]. The turbulence Prandtl number, Pr_t, is set to 0.85, and the turbulence Schmidt number, Sc_t, is set to 0.7.

Enhanced Wall Function – The above k-ε model is mainly valid for high Reynolds number fully turbulent flow. Special treatment is needed in the region close to the wall. The enhanced wall function is one of several methods that model the near-wall flow. In the enhanced wall treatment, the two-layer model is combined with the wall functions. The whole domain is separated into a viscosity-affected region and a fully turbulent region by defining a turbulent Reynolds number, Re_y,

$$Re_y = yk^{1/2}/\nu \tag{12}$$

where k is the turbulence kinetic energy and y is the distance from the wall. The standard k-ε model is used in the fully turbulent region where $Re_y > 200$, and the one-equation model of Wolfstein [25] is used in the viscosity-affected region with $Re_y < 200$. The turbulent viscosities calculated from these two regions are blended with a blending function (θ) to smoothen the transition.

$$\mu_{t,enhanced} = \theta\mu_t + (1-\theta)\mu_{t,l} \quad (13)$$

where μ_t is the viscosity from the k-ε model of high Reynolds number, and $\mu_{t,l}$ is the viscosity from the near-wall one-equation model. The blending function is defined so it is equal to 0 at the wall and 1 in the fully turbulent region. The linear (laminar) and logarithmic (turbulent) laws of the wall are also blended to make the wall functions applicable throughout the entire near-wall region.

Reynolds Stress Model – In film cooling, the interaction between the injected coolant flow and the approaching main flow could be anisotropic and nonequilibrium with multiscaled integral and dissipation length scales. Therefore, the Reynolds stress model (RSM), a second-moment closure, is considered in this study. The Reynolds stress transport equation can be given as

$$\frac{\partial}{\partial x_k}\left(\rho u_k \overline{u'_i u'_j}\right) = -\frac{\partial}{\partial x_k}\left[\rho u_k \overline{u'_i u'_j u'_k} + \overline{P(\delta_{kj}u'_i + \delta_{ik}u'_j)} + \mu\frac{\partial}{\partial x_k}\left(\overline{u'_i u'_j}\right)\right] - \rho\left(\overline{u'_i u'_k}\frac{\partial u_j}{\partial x_k} + \overline{u'_j u'_k}\frac{\partial u_i}{\partial x_k}\right) + \overline{P\left(\frac{\partial u'_i}{\partial x_j} + \frac{\partial u'_j}{\partial x_i}\right)} - 2\mu\overline{\frac{\partial u'_i}{\partial x_k}\frac{\partial u'_j}{\partial x_k}} \quad (14)$$

The diffusive term on the right-hand side can be modeled as

$$-\frac{\partial}{\partial x_k}\left[\rho u_k \overline{u'_i u'_j u'_k} + \overline{P(\delta_{kj}u'_i + \delta_{ik}u'_j)} + \mu\frac{\partial}{\partial x_k}\left(\overline{u'_i u'_j}\right)\right] = \frac{\partial}{\partial x_k}\left(\frac{\mu_t}{\sigma_k}\frac{\partial}{\partial x_k}\left(\overline{u'_i u'_j}\right)\right) \quad (15)$$

The second term on the right-hand side of Eq. (14) is the production term, and it is notated as G_{ij}

$$G_{ij} = -\rho\left(\overline{u'_i u'_k}\frac{\partial u_j}{\partial x_k} + \overline{u'_j u'_k}\frac{\partial u_i}{\partial x_k}\right) \quad (16)$$

The third term is the pressure-strain term, which can be modeled as

$$\overline{P\left(\frac{\partial u'_i}{\partial x_j} + \frac{\partial u'_j}{\partial x_i}\right)} = C_1\rho\frac{\varepsilon}{k}\left(\overline{u'_i u'_j} - \frac{2}{3}\delta_{ij}k\right) - C_2\left[A_{ij} - \frac{1}{3}\delta_{ij}A_{kk}\right] \quad (17)$$

where $A_{ij} = G_{ij} - \frac{\partial}{\partial x_k}\left(\rho u_k \overline{u'_i u'_j}\right)$. The constants C_1 and C_2 are 1.8 and 0.6, respectively. The last term in Eq. (14) can be approximated by

$$2\mu\overline{\frac{\partial u'_i}{\partial x_k}\frac{\partial u'_j}{\partial x_k}} = \frac{2}{3}\delta_{ij}\rho\varepsilon \quad (18)$$

and assumes this dissipation term isotropic.

Modeling of the turbulent heat flux and mass flux are similar as in the k-ε model. The turbulent kinetic energy and its dissipation rate can be calculated from the Reynolds stresses.

Other Models -- Ignoring details here, the turbulent models adopted in this study also include the RNG k-ε model, k-ω model, and the shear-stress transport (SST) k-ω model. RNG k-ε model was derived using renormalization group theory [26]. It has an additional term in the ε-equation to improve the accuracy for rapidly strained flows. It uses the effective viscosity to account for low-Reynolds-number effects. Theoretically, this model is more accurate and reliable than the standard k-ε model. The standard k-ω model is an empirical model based on transport equations for the turbulence kinetic energy (k) and the specific dissipation rate (ω), which can also be considered as the ratio of ε to k [27]. The low-Reynolds-number effect is accounted for in the k-ω model. The SST model is mixture of the k-ω model and the k-ε model: close to the wall it becomes the k-ω model while in the far field the k-ε model is applied [28].

Dispersed-Phase Model (Water Droplets)

Droplet Flow and Heat Transfer – Based on the Newton's 2nd Law, droplets motion in the airflow can be formulated by

$$m_p d\mathbf{v_p}/dt = \sum \mathbf{F} \quad (19)$$

where m_p is the droplet mass, and $\mathbf{v_p}$ is the droplet velocity (vector). The right-hand side is the combined force acted on the droplets, which normally includes the hydrodynamic drag, gravity and other forces such as the "virtual mass" force, thermophoretic force, Brownian force, and Saffman's lift force, etc.

Without considering the radiation heat transfer, droplet's heat transfer depends on convection and evaporation as given in the following equation.

$$m_p c_p \frac{dT}{dt} = \pi d^2 h(T_\infty - T) + \frac{dm_p}{dt}h_{fg} \quad (20)$$

where h_{fg} is the latent heat. The convective heat transfer coefficient (h) can be obtained with an empirical correlation [29-30]:

$$Nu_d = \frac{hd}{\lambda} = 2.0 + 0.6\,Re_d^{0.5}\,Pr^{0.33} \quad (21)$$

where Nu is the Nusselt number, and Pr is the Prandtl number.

The mass change rate or vaporization rate in Eq. (20) is governed by concentration difference between droplet surface and the air stream,

$$-\frac{dm_p}{dt} = \pi d^2 k_c (C_s - C_\infty) \quad (22)$$

where k_c is the mass transfer coefficient, and C_s is the vapor concentration at the droplet surface, which is evaluated by assuming the flow over the surface is saturated. C_∞ is the vapor concentration of the bulk flow, obtained by solving the transport equations. The values of k_c can be given from a correlation similar to Eq. (21) by [29-30].

$$Sh_d = \frac{k_c d}{D} = 2.0 + 0.6Re_d^{0.5}Sc^{0.33} \quad (23)$$

where Sh is the Sherwood number, Sc is the Schmidt number (defined as ν/D), and D is the diffusion coefficient of vapor in the bulk flow.

When the droplet temperature reaches the boiling point, the following equation can be used to evaluate its evaporation rate [31]:

$$-\frac{dm_p}{dt} = \pi d^2\left(\frac{\lambda}{d}\right)(2.0 + 0.46Re_d^{0.5})\ln\left(1 + c_p(T_\infty - T)/h_{fg}\right)/c_p \quad (24)$$

where λ is the gas/air heat conductivity, and c_p is the specific heat of the bulk flow.

Theoretically, evaporation can occur at two stages: (a) when the temperature is higher than the saturation temperature (based on local water vapor concentration), water evaporates, and the evaporation is controlled by the water vapor partial pressure until 100% relative humidity is achieved; (b) when the boiling temperature (determined by the air-water mixture pressure) is reached, water continues to evaporate. After the droplet evaporates due to either high temperature or low moisture partial pressure, the vapor diffuses into the main flow and is transported away.

Stochastic Particle Tracking - The turbulence effect on droplets dispersion is considered by using stochastic tracking. Basically, the

droplet trajectories are calculated by using the instantaneous flow velocity ($\bar{u}+u'$) rather than the average velocity ($\bar{u}$). The velocity fluctuations are then given as:

$$u' = \varsigma\left(\overline{u'^2}\right)^{0.5} = \varsigma(2k/3)^{0.5} \quad (25)$$

where ζ is a normally distributed random number [31]. This velocity will apply during the characteristic lifetime of the eddy (t_e), a time scale calculated from the turbulence kinetic energy and dissipation rate. After this time period, the instantaneous velocity will be updated with a new ζ value until a full trajectory is obtained. Note when the RSM model is used, the velocity fluctuation is independently decided in each direction.

Boundary Conditions

Continuous Phase – The main flow is assumed to be dry air (zero humidity). Uniform velocity (10 m/s) and temperature (400K) are assigned to the mainstream inlet. Coolant flow is assigned as saturated air (100% relative humidity). Without the plenum, jet inlet velocity of the coolant slot is 10 m/s, and the temperature is 300K. For cases with the plenum, the inlet velocity of coolant flow at the plenum inlet is 2.87 m/s, which gives an average jet velocity of 10 m/s. The inlet condition of the turbulence is specified by providing the turbulence intensity and the turbulence length scale (half of the hydraulic diameter times 0.07). The turbulent intensity of both mainstream inlet and coolant flow inlet is 1% for most of the cases, while a turbulent intensity of 10% is assigned to study its effect on cooling performance.

The flow exit (outlet) of main computational domain is assumed to be at a constant pressure. The backflow (reverse flow), if any, is set to 400 K. All the walls in the computational domain are adiabatic and have a non-slip velocity boundary condition.

Note that the above assigned temperature and velocity conditions are referenced in several previous studies of air-film cooling, for example [4] and [5], although they are not corresponding to the real conditions in gas turbine applications. For the convenience of comparing the results of this study to other published work, these values used by the previous published work are adopted in this study. While the current paper serves as a conceptual study on film cooling with mist injection, further research is to be performed with more realistic parameters for gas turbine applications.

Disperse Phase The droplet size is uniformly given as 10 μm. The mass ratio of mist over cooling airflow is 2%, which is about 7.0×10^{-4} kg/s for the 2-D slot with a unit depth of one meter. Mist is injected at 25 locations uniformly distributed along the jet inlet or the inlet of the air plenum. To examine the effect of the number of mist injection location, cases with different injection locations are considered. The effect of turbulent dispersion on droplet trajectories is calculated by tracking a number of trajectories with the stochastic method. The trajectory number is chosen to be 50 in most cases. Several test runs are conducted to check the effect of this trajectory number. The boundary condition of droplets at walls is assigned as "reflect", which means the droplets elastically rebound off once reaching the wall. At the outlet, the droplets just simply flee/escape from the computational domain. A more complex model is to be developed to determine if the droplets breakup, rebound, or are trapped by (or wet) the wall when they hit the wall.

Numerical Method

The commercial software package Fluent (version 6.2.16) from Fluent, Inc. is adopted in this study. The simulation uses the segregated solver, which employs an implicit pressure-correction scheme [32]. The SIMPLE algorithm is used to couple the pressure and velocity. Second order upwind scheme is selected for spatial discretization of the convective terms and species. Lagrangian trajectory calculations are employed to model the dispersed phase of droplets. The impact of droplets on the continuous phase is considered as source terms to the governing equations. After obtaining an approximate flow field of the continuous phase (airflow in this study), droplets are injected and their trajectories are calculated. At the same time, drag, heat and mass transfer between the droplets and the airflow is calculated.

As shown in Fig. 2, structured but nonuniform grids are constructed in this study. The grids near the jet wall and the bottom wall of the main domain are denser than the other area. The grid number is 400 in the x-direction and 120 in the y-direction. Different meshes are tested for grid dependence. Furthermore, the near-wall grid is adapted twice to test its effect on calculated results for both single-phase and mist film cooling cases.

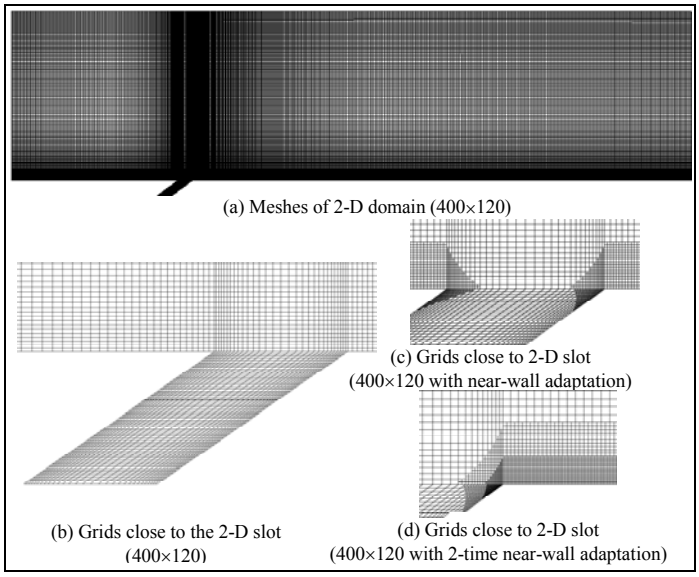

Figure 2 Meshes

Iteration proceeds alternatively between the continuous and discrete phases. Ten iterations in the continuous phase are conducted between two iterations in the discrete phase. Converged results are obtained after the specified residuals are met. A converged result renders mass residual of 10^{-4}, energy residual of 10^{-6}, and momentum and turbulence kinetic energy residuals of 10^{-5}. These residuals are the summation of the imbalance for each cell, scaled by a representative of the flow rate. Typically, 1000 to 2000 iterations are needed to obtain a converged result, which takes about 1~2 hours on a 2.8 GHz Pentium 4 personal computer.

Results and Discussion

Baseline Case

The baseline case is run with the basic mesh (400×200) shown in Fig. 2 (a). The inlet velocity is 10 m/s for both the mainstream and jet flow. The temperatures are 400 and 300 K for the mainstream and jet flow, respectively. Considering the density difference, the blowing ratio, defined as $M=(\rho u)_c/(\rho u)_g$, is 1.3 in this case, while the ratio of velocity is 1. Here the subscript "c" represents the coolant flow, and "g" represents the main flow. The standard k-ε turbulence model with

enhanced wall treatment is used with an inlet turbulence intensity of 1%. Mist mass ratio is 2%, and the droplet size is 10-μm. The mist is injected into the jet flow uniformly at 25 locations of the inlet. Stochastic tracking is used with a trajectory number of 50. Therefore, the total number of trajectories is 1250 (50×25).

The adiabatic cooling effectiveness (η) is used to examine the performance of mist film cooling. The definition of η is:

$$\eta = (T_g - T_{aw})/(T_g - T_c) \quad (26)$$

where T_g is the mainstream hot gas temperature, T_c is the temperature of the coolant (jet), and T_{aw} is the adiabatic wall temperature. η ranges from 0 (no cooling) to 1 (ideal case). Figure 3 shows the effectiveness along the cooling surface. Note that the hydraulic diameter of the slot (2b) is used to scale the distance downstream. It can be seen that film cooling is significantly enhanced by mist injection, especially in the downstream region, where the evaporation of droplets becomes stronger because of deterioration of air film cooling and the resulted higher flow temperature. Due to continuous mixing between the main flow and coolant, film cooling inevitably becomes less effective downstream. It has been a serious challenge to enhance cooling downstream of x/2b=15. The injection of water droplets works very well to meet this challenge. Also shown in Fig. 3 is the cooling enhancement ratio with and without mist (η_{mist}/η_0). The cooling enhancement can be defined as (η_{mist}/η_0-1). It can be seen that the maximum enhancement can reach 42% further downstream (x/2b=30) with an average cooling enhancement of 15.5%.

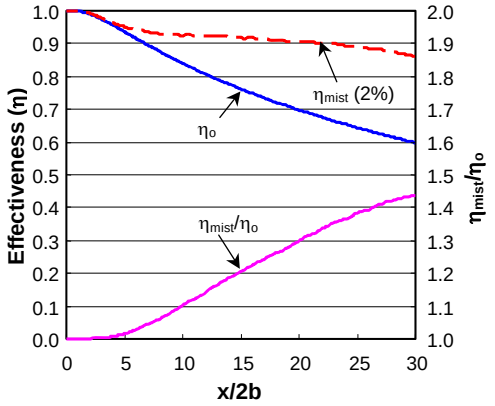

Figure 3 Baseline cooling effectiveness and enhancement

Effect of Near-Wall Grid

To apply the enhanced wall treatment in resolving the viscosity-affected near-wall region, the near-wall mesh should be constructed to have y^+ at the order of 1. It is also reported that a higher y^+ is acceptable as long as it is well inside the viscous sublayer ($y^+ < 4$ to 5). Figure 4 shows the y^+ value along the wall in the current study. It can be seen that y^+ ranges from 3~4.5 for the basic grid. The y^+ value of film cooling with mist is almost the same as the case without mist. To examine the effect of the near-wall grid on mist film cooling simulation, the near-wall grid is refined twice – each time the density of 10 grids close to the wall are doubled in both directions: The first doubling brings the y^+ value to 1.5~2, and the second doubling makes the y^+ value lower than 1 at most of the locations.

The effect of near-wall grids on film cooling is shown in Fig. 5. The results of all the three single-phase film cooling cases show identical values. This indicates that the first near-wall grid could be placed at $y^+ = 5$ and do not affect the results for the air-film cases. As to the mist film cooling, there is a 3~5 percentage points increase of the cooling effectiveness when the finer grids are adopted. A possible reason is that the source terms contributed by droplet evaporation become more important to smaller control volumes near the wall. The low velocity close to the wall keeps the droplets in the viscous layer longer. Evaporative cooling is more effective near the wall because the droplets are physically present near the wall when finer near-wall grids are present in the computational domain. However, the wall function treatment could represent the velocity profile adequately but does not include the discrete phase if no-grids are present near the wall.

Due to the low velocity close to the wall, more time steps are needed to calculate the droplets' trajectories and the CPU time increases significantly (3~5 times).

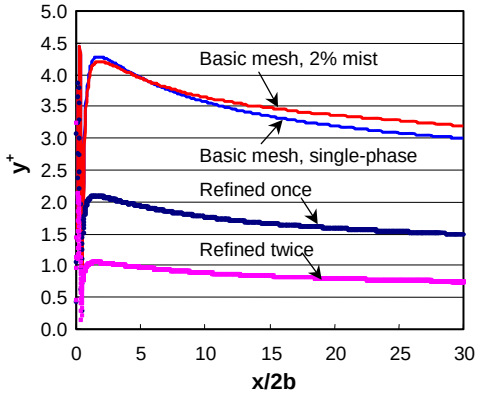

Figure 4 y^+ along the wall with different grid systems

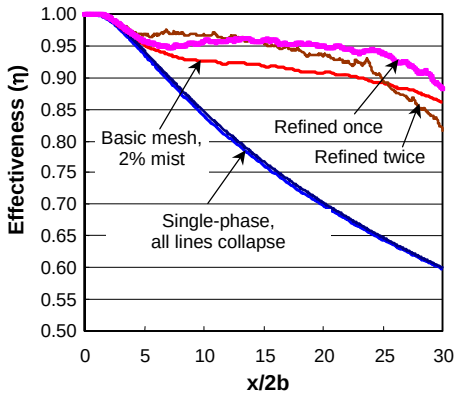

Figure 5 Cooling effectiveness with different grid systems

Effect of Turbulence Models

To study the effect of turbulence models on film cooling simulation, different turbulence models, including the RNG k-ε, k-ω, and Reynolds stress model, are employed. Figure 6 shows the cooling effectiveness from different models. Basically, the standard k-ε, RNG, and RSM models give very similar results: The cooling effectiveness differs only by 0.02, which is slightly higher than the test data in [33]. However, the k-ω and SST give results significantly deviating from the former group; the difference of cooling effectiveness can be as large as 0.2. The extremely high cooling effectiveness could indicate either a large downstream separation occurs or a very low mixing or diffusion rate is calculated in terms of low turbulence viscosity. Further analysis shows that the flow structure near the jet exit also varies with the turbulence model used. It is speculated that the

different flow patterns predicated by various turbulence models could shed some light on explaining the different cooling performance. Figure 7 shows that the standard k-ε model predicts a small recirculation region induced by flow separation downstream the jet, while all the other models, including both the SST model and RSM model, predict a larger flow separation. Since both RNG and RSM predict similar cooling performance as the standard k-ε model, the effect of the different sizes of separation region seem to not be predominant on cooling effectiveness in this study. An even smaller vortex located immediately upstream of the jet exit is predicted. Its effect on cooling effectiveness could be ignored. The downstream separation is expected to exert a negative impact on aerodynamic efficiency.

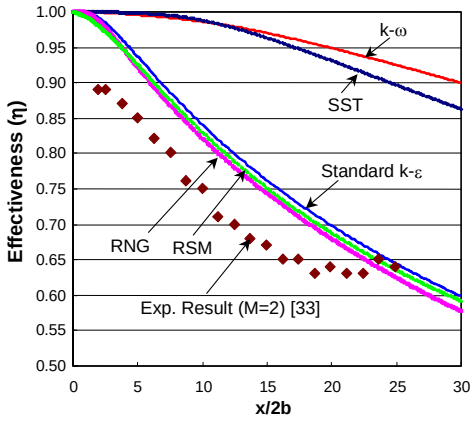

Figure 6 Effect of turbulence models on single-phase film cooling performance

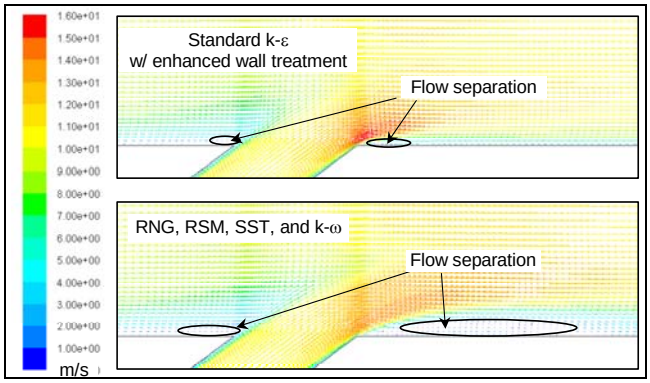

Figure 7 Flow field close to the jet exit predicted by different turbulence models

Figure 8 shows the effect of turbulence models on mist film cooling. Since both the k-ω and SST models could not predict a reasonable result for single-phase film cooling, these two models are not applied for mist cooling cases. The RNG model gives a similar result as the standard k-ε model does. The cooling effectiveness result of RSM model is consistently lower than the other two turbulence models by 0.05. The explanation can be sought by looking into the prediction of turbulence characteristics in Figs. 9 and 10.

Figure 9 shows the distribution of the Reynolds stresses in contour plots, and Fig. 10 presents the Reynolds stress values at y/2b = 0.125. As expected, the turbulence is anisotropic near the jet exit and the adiabatic wall. The Reynolds stress of $\overline{u'u'}$ is larger than $\overline{v'v'}$ in most cases, and even far downstream the anisotropy index (ratio of $\overline{u'u'}$ and $\overline{v'v'}$) can be as high as 5. Compared to other models, RSM predicts smaller turbulence fluctuations in the y-direction, and that makes the droplets move at a lower speed towards the wall. Therefore, the droplets effect predicted by RSM model becomes relatively weaker. The Reynolds stresses become very small in the field far away from the wall (not shown in the figure), and the ratio of Reynolds stresses ($\overline{u'u'}$ / $\overline{v'v'}$) is close to 1, which means the flow is close to isotropic in the far field. Rigorous turbulence transport, represented by the value of $\overline{u'v'}$, seems to present in the region of x/2b<5 as shown in Fig. 10.

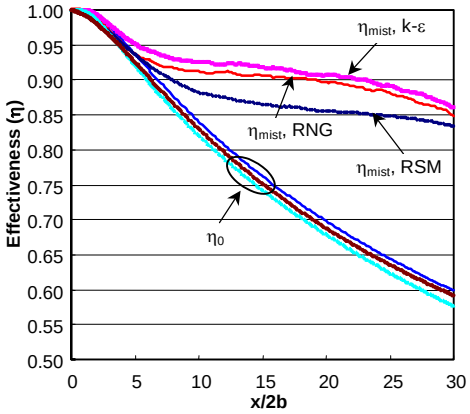

Figure 8 Effect of turbulence models on mist film cooling performance

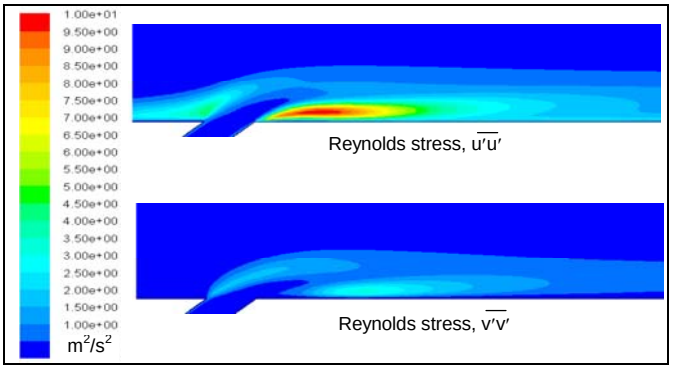

Figure 9 Distribution of Reynolds stresses close to the jet exit predicted by the RSM model

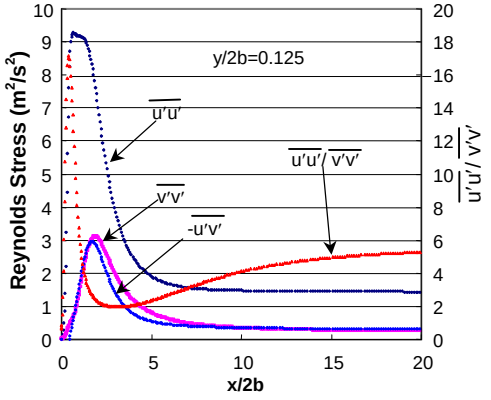

Figure 10 Reynolds stresses predicted by the RSM model

Effect of the Number of Injection Locations

In a real application, the droplets are expected to be premixed uniformly in the coolant before entering the plenum. In simulation, the droplets are uniformly injected into the flow from a limited number of locations with a specified flow rate. It is understandable that the simulation results will be more accurate when more injection locations are applied in simulation. However, more injection locations will require more computational time. To examine how the injection number affects the numerical results, Fig. 11 shows the effect of three different injection numbers on the cooling effectiveness. The results show that the average cooling effectiveness is similar for all the three injection numbers. The smaller injection number at 10 has caused unrealistic numerical jiggles. The highest injection number at 100 locations gives the smoothest cooling effectiveness distribution. To save computational time, injection number at 25 locations is selected for all cases because the overall results are sufficiently comparable within one percentage point to that predicted by employing 100 injection locations.

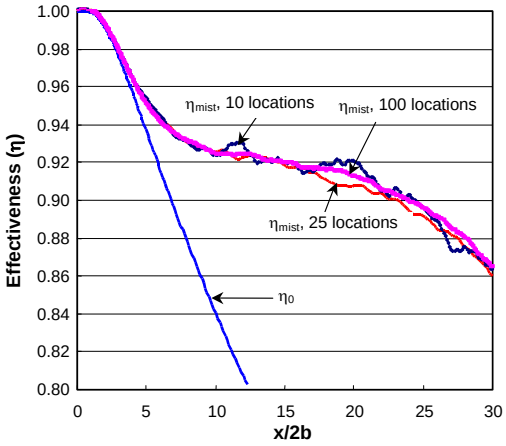

Figure 11 Effect of number of injection locations

Effect of Number of Stochastic Tracking

To take into account the effect of turbulence on the dispersion of droplets by using stochastic tracking scheme, trajectories are calculated and traced multiple times for each droplet injection and the averaged effect is applied to the main flow. It is desirable to know how many times the trajectories should be traced and how important the turbulence dispersion is on mist film cooling. Figure 12 shows the results with different tracking numbers. Without random tracking, the effectiveness of mist film cooling is about 10 percentage points lower because all the droplets follow the streamline closely and theoretically never have a chance to move closer or touch the wall. The instantaneous, unsteady droplet dynamics induced by instantaneous turbulence fluctuations is not included in the Reynolds average equation. Random tracking scheme creates a distributed random number to simulate the instantaneous random turbulence fluctuations and apply the random fluctuations to droplets only (see Eq. 25). The turbulence calculation is not affected. Although the droplets' trajectory is not the same as the streamline, they are very close when the droplet size is small. By considering the turbulence dispersion, the droplets derivate from the streamline and some of them move towards the surface, leading to a significantly increased effectiveness downstream of x/2b=5. The random effect of the turbulence on the droplets can be reasonably predicted only if a sufficient number of trajectories are calculated. Fewer trajectories will show a non-smooth distribution of the effectiveness, which does not correctly reflect the actual effect from numerous droplets. In this study, the trajectory number for the baseline case is chosen to be 50 at each injection location. The total trajectory number is 50×25=1250, which gives a reasonable smooth curve.

It should be noted that the iteration convergence becomes difficult after introducing the stochastic tracking, especially with a small number of trajectories. As seen in Fig. 13, after activating the mist injection, the residuals drop first, followed by fluctuation at a certain level. The fluctuation does not exist in the case of mist film cooling without stochastic tracking. This is because with stochastic tracking, the trajectories change each time the discrete phase information is updated and the source terms contributed by the droplets change accordingly, even though the flow field of continuous phase keeps the same. Therefore, the residuals increase each time the droplets are re-tracked. Tracking more trajectories from a large number of injections reduces the level of residuals fluctuations.

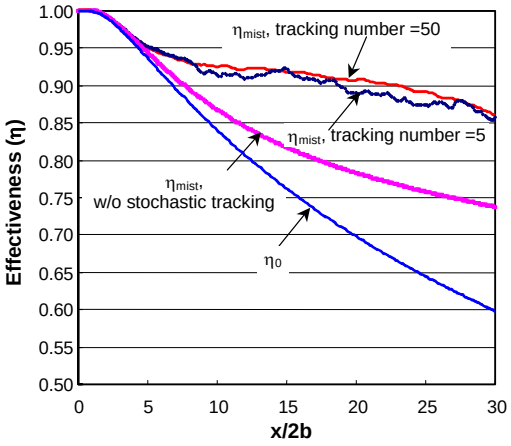

Figure 12 Effect of number of stochastic tracking

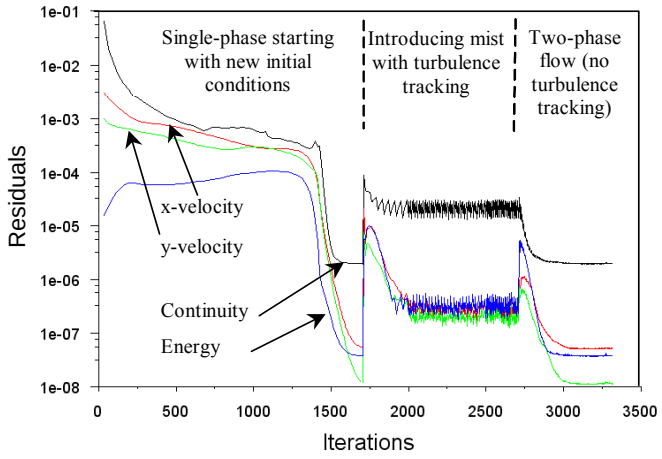

Figure 13 Residual histories

Effect of Inlet Turbulence Intensity

Figure 14 presents the effect of inlet turbulence intensity between 1% and 10%. Four cases have been conducted: 1% for both main flow and jet flow; 1% for main flow and 10% for jet flow; 10% for main flow and 1% for jet flow; and 10% for both main and jet flow. Higher turbulence intensity reduces the cooling effectiveness due to a higher mixing rate between the main flow and coolant. The maximum reduction of cooling effectiveness is about 0.05 under the conditions of

this study. It is found that the coolant inlet turbulence intensity mainly affects the cooling performance close to the jet exit and the main flow inlet turbulence intensity affects the result far downstream. As to the mist film cooling, the higher inlet turbulence intensity enhances the mixing of the coolant and main flow, but at the same time it can augment the droplet turbulence dispersion towards the wall. The combined effect produces a little bit lower cooling effectiveness (0.01~0.02) in this study, which is also shown in Fig. 14.

Mayhew et al. [9] reported that higher jet inlet turbulence intensity produces a lower cooling effectiveness when the blowing ratio is low (0.5). However, at high blowing ratio (1.5), higher jet inlet turbulence intensity helps bring the coolant towards the wall and improves the cooling performance. The cases in [9] are for three-dimensional holes, and the 3-D effect can contribute to this difference.

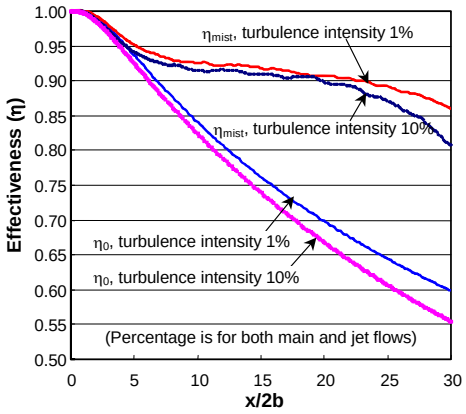

Figure 14 Effect of inlet turbulence intensity

Effect of Inlet Plenum

Several numerical studies, for example, [5] and [9], included a plenum with different flow arrangements to account for the effect of flow entering the jet hole on film cooling. They reported that the plenum geometry could largely affect film cooling flow pattern and cooling performance. The effect of plenum is also examined for mist film cooling in this study. The plenum has a size of 7.0b×3.5b, and its inlet is parallel to the main flow.

As shown in Fig. 15, under the parameters of the current study, the plenum does play an important role for both the single-phase and mist film cooling. With the plenum considered, the effectiveness decreases by 0.03~0.04 for single-phase and 0.07~0.1 for mist film cooling, respectively. Figure 16 gives the details of flow fields close to the injection slot. It can be seen that the flow separates inside the coolant supply passage. The turbulence intensity of the coolant flow increases significantly due to flow separation inside the film slot. The high turbulence results in reduced cooling effectiveness due to a rapid mixing between the coolant and main flow. As seen in the Fig. 16, the droplets trajectories significantly deviate from the case without the plenum. When the turbulence dispersion is not considered by applying stochastic tracking, all the droplets tend to merge into a finite string after leaving the plenum, which is the typical "roping" phenomenon. The turbulent fluctuation can make the droplets "string" loosened. However, compared to the case without plenum, the average trajectory of the droplets moves away from the cooling wall, which degrades the cooling performance. The effect of plenum on mist film cooling performance is more than on single-phase film cooling performance. More studies are needed to determine optimizing plenum geometries for mist film cooling applications.

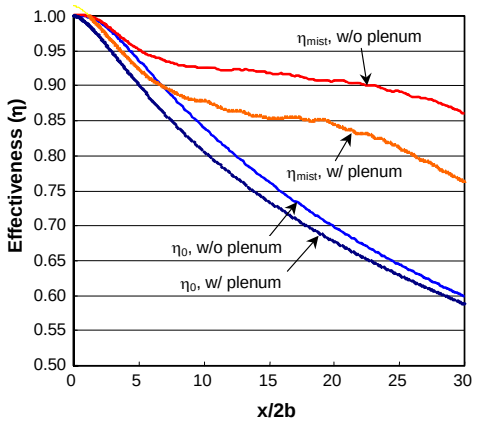

Figure 15 Effect of inlet plenum on film cooling performance

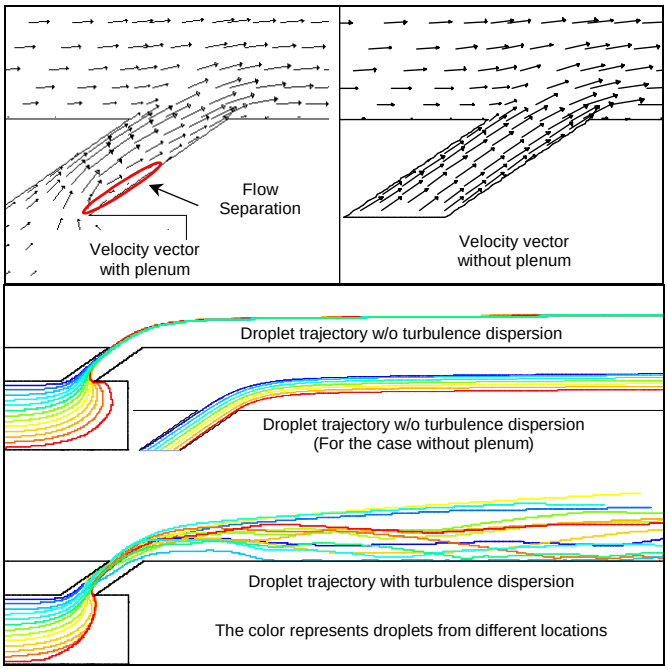

Figure 16 Velocity vector and droplet trajectories near the jet slot with inlet plenum for mist film cooling

Effect of Saffman Lift, Thermophoretic and Brownian Forces

Recognizing that the motion of droplets in film cooling is subject to additional forces such as Thermophoretic force, Saffman lift, and Brownian force, cases are run to investigate the importance of these forces with one force exclusively activated each time. Saffman force [34] concerns a sphere moving in a shear field. It is perpendicular to the direction of flow, originating from the inertia effects in the viscous flow around the particle. It can be given as

$$F_{saff} = 1.615\rho\nu^{0.5}(u_g - u_p)(du/dn)^{0.5} \quad (26)$$

where du/dn is the gradient of the tangential velocity. It is valid only when $Re_p \ll 1$.

The thermophoretic force is arisen from asymmetrical interactions between a particle and the surrounding fluid molecules due to a temperature gradient. This force tends to repel particles or

droplets from a high temperature region to a low temperature region. The following equation can be used to model this force.

$$F_n = -K\frac{1}{m_p T}\frac{\partial T}{\partial n} \quad (27)$$

Where K is a thermophoretic coefficient, and more details can be found in Talbot et al. [35]

Brownian force is to consider the random motion of a small particle suspended in a fluid, which is resulted from the instantaneous impact of fluid molecules. It can be modeled as a Gaussian white noise process with spectral intensity given by [36]

Results indicate that the effect of Saffman lift and Brownian force is imperceptible. The Thermophoretic force, which tends to move the droplets towards the cold wall, increases the cooling effectiveness by 0.01 on average. Since all the curves collapse into the baseline case, no figure is given here.

Concerns and Future Research

The main objective of this study is to explore the concept of mist film cooling and disparity induced by applying various models and schemes on mist film cooling simulation. Although numerical simulation shows promising results by employing mist film cooling, experimental studies are needed to verify these simulated results. Once the experimental data are available, numerical models will be modified. For example, the interaction of droplet with heated wall could be more complicated than the simple reflection applied in this study. The importance of droplet collision and coalescence could be evaluated in the future studies. There is a concern on the potential erosion and corrosion introduced by the water droplets on the gas turbine airfoils. This concern needs to be investigated before implementing the mist film cooling scheme.

Conclusions

By injecting a small amount of droplets (mist) into the cooling air, the performance of film cooling could be improved significantly. This paper conducts numerical simulation to explore this new concept, focusing on the effect of turbulence models, and numerical modeling schemes of the dispersed-phase. The effects of inlet turbulence intensity as well as the grid density on numerical results are also studied. The conclusions are:

- Injecting 2% mist into the coolant can increase the cooling effectiveness downstream about ~ 45%.
- Near-wall grids within a y^+ of 5 show little effect on the single-phase film cooling result. Refined grids close to the wall are needed to provide more accurate predictions for mist film cooing.
- Results given by the RNG k-ε model, RSM, and the standard k-ε model with enhanced wall treatment are consistent. Both the k-ω and SST models show unrealistic high cooling effectiveness. RSM model shows that the lower normal Reynolds stress ($\overline{v'v'}$) in the y-direction results in a lower cooling effectiveness than other turbulence models.
- The turbulence dispersion shows a significant effect on mist film cooling by using the stochastic tracking scheme. Approximately 10 percentage points cooling effectiveness enhancement are resulted in addition to the enhancement from the mist film cooling without considering turbulence dispersion. Random tracking makes the calculation convergence difficult. Adequate cooling effectiveness distribution can be obtained with calculation of 50 or more trajectories at each injection locations.
- 25 injection locations of droplets are enough to catch the effect of the mist on film cooling in this study. Numerical jiggles on the cooling effectiveness curve appear when fewer injection locations are employed.
- Increasing the inlet turbulence intensity from 1% to 10% gives a 5 percentage points decrease of cooling effectiveness in this study. The effect of inlet turbulence intensity on single-phase and mist film cooling is similar.
- The plenum changes the coolant velocity profile and turbulence intensity at the injection slot exit. The cooling performance is adversely affected when the plenum is included in this study due to a flow separation in the film slot and roping phenomenon of droplets.
- The cooling effectiveness increases by 1 percentage point on average when the thermophoretic force is included, which tends to move the droplets towards the wall. The effect of Brownian force and Saffman lift is imperceptible.

Acknowledgement

This study is partially supported by the Louisiana Governor's Energy Initiative via the Clean Power and Energy Research Consortium (CPERC) and administered by the Louisiana Board of Regents.

References

[1] Eriksen, V.L. and Goldstein, R. J., 1974, "Heat Transfer and Film Cooling Following Injection Through Inclined Tubes," ASME J. Heat Transfer, **96**, pp. 239–245.

[2] Goldstein, R. J., Eckert, E. R. G., and Burggraf, F., 1974, "Effects of Hole Geometry and Density on Three-Dimensional Film Cooling," Int. J. Heat Mass Transfer, **17**, pp. 595–607.

[3] Jia, R., Sunden, B., Miron, P., and Leger, B., 2003, "Numerical and Experimental Study of the Slot Film Cooling Jet with Various Angles," Proceedings of the ASME Summer Heat Transfer Conference, pp. 845-856.

[4] Bell, C. M., Hamakawa1, H., and Ligrani, P. M., 2000, "Film Cooling From Shaped Holes," ASME J. Heat Transfer, **122,** pp. 224-232.

[5] Brittingham, R.A. and Leylek, J. H, 2002, "A Detailed Analysis of Film Cooling Physics: Part IV—Compound-Angle Injection with Shaped Holes," ASME J. Turbomachinery, **122,** pp. 133-145.

[6] Taslim, M.E, and Khanicheh, A., 2005, "Film Effectiveness Downstream of a Row of Compound Angle Film Holes," ASME J. Heat Transfer, 127, pp. 434-439.

[7] Kwak, J. S. and Han, J. C., 2003, "Heat Transfer Coefficients and Film-Cooling Effectiveness on a Gas Turbine Blade Tip," ASME J. Heat Transfer, **125,** pp. 494-502.

[8] Mayhew, J. E., Baughn, J. W., and Byerley, A. R., 2004, " Adiabatic Effectiveness of Film Cooling with Compound Angle Holes-The Effect of Blowing Ratio and Freestream Turbulence," ASME J. Heat Transfer, 126, n. 4, pp. 501-502.

[9] Adami, P., Martelli, F., Montomoli, F., and Saumweber, C., 2002, "Numerical Investigation of Internal Crossflow Film Cooling," ASME Turbo Expo 02, **3A**, pp. 51-63.

[10] Wang, T., Chintalapati, S., Bunker, R. S., and Lee, C. P., 2000, "Jet Mixing in a Slot," Experimental Thermal and Fluid Science, **22**, n. 1, pp. 1-17.

[11] Chaker, M., Meher-Homji, C.B., and Mee, M., 2002, "Inlet Fogging of Gas Turbine Engines - Part A: Fog Droplet

Thermodynamics, Heat Transfer and Practical Considerations," ASME Proceedings of Turbo Expo 2002, **4**, pp. 413-428.
[12] Petr, V., 2003, "Analysis of Wet Compression in GT's," Energy and the Environment - Proceedings of the International Conference on Energy and the Environment, **1**, pp. 489-494.
[13] Nirmalan, N. V., Weaver, J. A., and Hylton, L. D., 1998, "An Experimental Study of Turbine Vane Heat Transfer with Water–Air Cooling," ASME J. Turbomachinery, **120**, No. 1, pp. 50–62.
[14] Guo, T., Wang, T., and Gaddis, J. L., 2000, "Mist/Steam Cooling in a Heated Horizontal Tube, Part 1: Experimental System, Part 2: Results and Modeling," ASME J. Turbomachinery, **122**, pp. 360–374.
[15] Guo, T., Wang, T., and Gaddis, J.L., 2001, "Mist/Steam Cooling in a 180^o Tube Bend," ASME J. Heat Transfer, **122,** pp. 749-756.
[16] Li, X., Gaddis, J. L., and Wang, T., 2003, "Mist/Steam Cooling by a Row of Impinging Jets," Int. J. Heat Mass Transfer, **46**, pp. 2279-2290.
[17] Li, X, Gaddis, J. L., and Wang, T, " Mist/Steam Heat Transfer with Jet Impingement onto a Concave Surface," ASME J. Heat Transfer, vol. 125, pp. 438-446
[18] Heidmann, J. D., Rigby, D. L. and Ameri, A. A., 2000, "A Three-Dimensional Coupled Internal/External Simulation of a Film-Cooled Turbine Vane," ASME J. Turbomachinery, **122**, pp. 348-359.
[19] Tyagi, Mayank, and Acharya, Sumanta, 2003, "Large Eddy Simulation of Film Cooling Flow from an Inclined Cylindrical Jet," ASME J. Turbomachinery, **125**, n. 4, pp. 734-742.
[20] Wang, M. J. and Mayinger, F., 1995, "Post-dryout Dispersed Flow in Circular Bends," Int. J. Multiphase Flow, **21**, n. 3, pp. 437-454.
[21] Aggarwal, S.K. and Park, T.W., 1999, "Dispersion of Evaporating Droplets in a Swirling Axisymmetric Jet," AIAA Journal, **37**, n. 12, pp. 1578-1587.
[22] Chen, X.-Q. and Pereira, J.C.F., 1995, "Prediction of Evaporating Spray in Anisotropically Turbulent Gas Flow," Numerical Heat Transfer; Part A: Applications, **27**, n. 2, pp. 143-162.
[23] Li, X and Wang, T., 2005, "Simulation of Film Cooling Enhancement with Mist Injection," ASME Turbo Expo 2005, Nevada, USA, June 6-9.
[24] Launder, B. E. and Spalding, D. B., 1972, Lectures in Mathematical Models of Turbulence, Academic Press, London, England.
[25] Wolfstein, M., 1969, "The Velocity and Temperature Distribution of One-Dimensional Flow with Turbulence Augmentation and Pressure Gradient," Int. J. Heat Mass Transfer, **12,** pp. 301-318.
[26] Choudhury, D., 1993, Introduction to the Renormalization Group Method and Turbulence Modeling, Technical Memorandum, TM-107, Fluent Inc.
[27] Wilcox, D.C., 1998, Turbulence Modeling for CFD, DCW Industries, Inc., La Canada, California.
[28] Menter, F, 1993, "Zonal Two Equation Model for Aerodynamic Flows," AIAA Paper 93-2906.
[29] Ranz, W. E. and Marshall, W. R. Jr., 1952, "Evaporation from Drops, Part I," Chem. Eng. Prog., **48**, pp. 141-146.
[30] Ranz, W. E. and Marshall, W. R. Jr., 1952, "Evaporation from Drops, Part II," Chem. Eng. Prog., **48**, pp. 173-180.
[31] Kuo, K. Y., 1986, Principles of Combustion, John Wiley and Sons, New York.
[32] Fluent Manual, Version 6.2.12, 2005, Fluent, Inc.
[33] Rhee, D. H., Lee, Y. S. and Cho, H. H, 2002, "Film Cooling Effectiveness and Heat Transfer of Rectangular-shaped Film Cooling Holes," ASME Turbo Expo, **3**, pp. 21-32.
[34] Saffman, P.G., 1965, "The Lift on a Small Sphere in a Slow Shear Flow," J. Fluid Mech., **22,** pp. 385-400.
[35] Talbot, L. Cheng, R. K., Schefer, R. W., and Willis, D. R., 1980, "Thermophoresis of Particles in a Heated Boundary Layer," J. Fluid Mech., **101**, pp.737-758.
[36] Li, A. and Ahmadi, G., 1992, "Dispersion and Deposition of Spherical Particles from Point Sources in a Turbulent Channel Flow," Aerosol Science and Technology, 16, pp. 209-226.